



# A predefined-time radial basis function (RBF) neural network tracking control method considering actuator faults for a new type of spraying robot

Jingang Zhao<sup>1,2</sup>, Yinghui Li<sup>2</sup>, Yiwu Li<sup>1,2</sup>, Binbin Pei<sup>1</sup>, Zhilong Yu<sup>2</sup>, and Zehong Dong<sup>3</sup>

<sup>1</sup>National Key Lab of Aerospace Power System and Plasma Technology,  
Air Force Engineering University, Xi'an 710038, China

<sup>2</sup>Aviation Engineering School, Air Force Engineering University, Xi'an 710038, China

<sup>3</sup>High Speed Aerodynamics Research Institute, China Aerodynamics Research  
and Development Center, Mianyang 621000, China

**Correspondence:** Yiwu Li (lee\_yiwu@163.com)

Received: 7 August 2024 – Revised: 22 September 2024 – Accepted: 2 November 2024 – Published: 24 January 2025

**Abstract.** A small-range fine-spraying collaborative robot (SFSC) for vehicle surface repair has been designed, which has 4 degrees of freedom. Conventional control methods, such as sliding mode control (SMC) have difficulty meeting the accuracy requirements when the end of the attitude adjustment robotic arm control is spraying. Focusing on the problem of tracking control of a multi-joint robot with uncertain information, such as modeling uncertainty and random interference, a predefined-time radial basis function (RBF) neural network tracking control (PRC) method considering actuator fault is proposed for a new spraying robot. Firstly, the dynamics equations of the  $n$ -joint manipulator are derived using the Euler–Lagrange equation. Then, a new predefined-time sliding mode surface is designed based on the stability theory of PRC. Combined with the Euler–Lagrange dynamics model of the two-joint manipulator, a nonsingular PRC controller is designed according to the uncertainty in model parameters and external interference. Stability of the system is proven based on Lyapunov theory. The simulation results show that the designed controller can ensure that the state convergence of the system does not depend on the initial conditions and has a faster convergence rate, shorter convergence time and good robustness.

## 1 Introduction

The multi-joint robot is a very complex multi-input and multi-output nonlinear system, which has the dynamic characteristics of time variability, coupling and nonlinearity (Spong et al., 2020). How to effectively track and control the uncertain robot system has been the focus of robot control algorithm research (Lynch and Park, 2017). A high-quality robot control algorithm must take into account various factors of uncertainty, including modeling errors, uncertain disturbances and actuator failures, so that the machine has the ability to actively adapt to environmental disturbances and controlled system motion changes.

Automatic spraying robots can cleanly and efficiently complete a variety of spraying operations and are widely

used in automotive, aircraft, furniture spraying and other fields. Yu et al. (2018) of Tsinghua University proposed the use of a moving guide rail in the form of a gantry frame combined with inverted spraying robot for spraying aircraft. Morelli et al. (2018) installed the spraying robot on the automated guided vehicle (AGV) with lifting platform, achieving the spraying task of large workpieces, such as aircraft spraying operations, by increasing the degrees of freedom of the spraying robot base. These methods use robotic arms with spray guns attached to them, but the problem with this is that the inertia of the system increases with the increase in the arm length or the number of joints of the robot arm, resulting in a decrease in the accuracy of its end (Zhang et al., 2020; Liu et al., 2023; Chen et al., 2020).

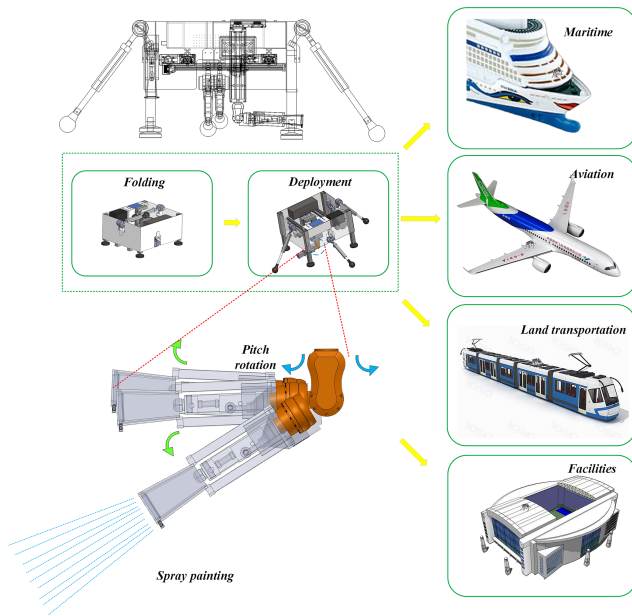


Figure 1. SFSC for vehicle surface repair.

Based on the above problems, a small-range fine-spraying collaborative robot (SFSC) with 4 degrees of freedom was designed for vehicle surface repair, and the spraying operation was replicated by force guidance and teaching. The SFSC is a semi-automatic instrument that assists with manual operation which can be folded for easy transportation. Its status of folding volume is  $0.25 \text{ m}^3$ , status of deployment volume is about  $0.75 \text{ m}^3$  and weight is 20.35 kg. Its spray gun is located at the bottom of the machine and can be placed on the upper side of the area to be sprayed for work. Therefore, the SFSC can be applied in spraying not only military vehicles such as aircraft, ships and submarines, but also for civil purposes such as construction and vehicle spraying and even that of electrical appliances and furniture.

The SFSC can implement self-awareness, self-learning, self-execution and self-adaptation by writing control algorithms such as reinforcement learning, genetic algorithm (GA) and generative adversarial networks (GAN) (Yang et al., 2023).

However, in the process of spraying operation, the spraying trajectory of the SFSC has a regular deviation from the ideal state. After the problems of the mobile mechanism were eliminated, it was found that the angular position accuracy of the posture adjustment mechanism produced considerable errors when applying traditional control methods. In order to solve the control precision problem of the robot spraying operation, the PRC method considering actuator fault for the SFSC was proposed.

Predefined-time tracking control has been widely used in the design of control systems, including high-order integrator systems (Becerra et al., 2018) and multi-agent systems (Li et al., 2021). Munoz-Vazquez et al. (2019) designed the

predefined-time robust controller of the robot system, considering its model uncertainty, which is based on the inherent dynamics analysis model characteristics of the robot. However, its limitation is that the performance of the controller is very sensitive to parameter selection, and finding the optimal parameter may require a complex debugging process. C. Wang et al. (2024) proposed an adaptive fuzzy tracking control method with predefined-time and precision for strict feedback nonlinear systems. Based on the criterion, an adaptive fuzzy controller is designed which can prescribe the stability time and convergence accuracy of the tracking error. Pan et al. (2023) proposed a predefined-time adaptive neural tracking control problem for nonlinear multi-agent systems (MASs) using neural networks (NNs) and finite-time differentiators. However, the limitations of these methods were that they increased the dependence on the initial value of the system. Ye et al. (2021) proposed an attitude tracking control method for rigid spacecraft with limited external disturbances, which is based on a nonsingular predefined-time sliding mode manifold for predefined-time bounded attitude tracking control.

This paper focuses on the PRC method for unknown Euler–Lagrange systems with actuator faults and any bounded initial value. The attitude adjustment mechanism of the self-designed spraying robot is equivalent to a two-joint cooperative robot system. Taking the rotating component of this design as the simulation object, quality, rod length and other conditions are substituted into the simulation system to verify the effectiveness of the method.

The main features of this paper can be roughly summarized as follows:

1. By means of error transformation, the preset performance function of specified time is introduced into the controller design so as to ensure the synchronous adjustment of convergence accuracy and convergence speed.
2. Unlike existing prescribed performance control (PPC) (Lai et al., 2024; Tang and Zhao, 2017), whose controllers need to be designed according to the initial values of the system, the shift function is refined and introduced to ensure that the proposed control algorithm is independent of the initial value of the system in this paper, thus eliminating the above limitations.
3. The control algorithm is applied to the self-designed robot device to solve the steady-state error problem of the robot device.

## 2 Question description

### 2.1 Attitude adjustment problem of the SFSC

The overall structure of the SFSC is shown in Fig. 2. During operation, the system controlled the linear movement of the

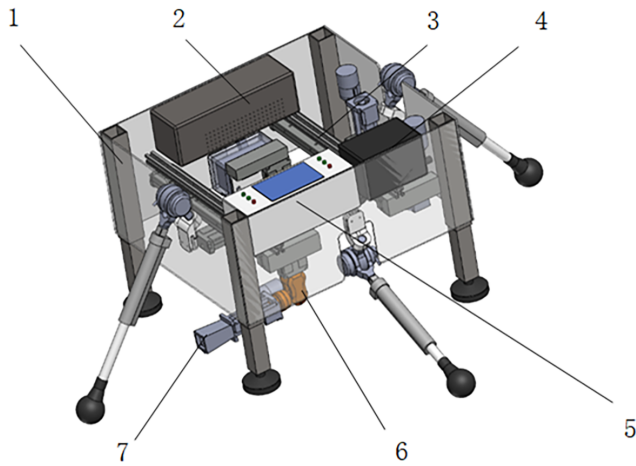


**Figure 2.** Overall structure of the SFSC. 1: frame mechanism, 2: electric gas source device, 3: displacement mechanism, 4: protection components, 5: industrial computer, 6: attitude adjustment mechanism and 7: spray gun mechanism.

$x$ ,  $y$  and  $z$  axes in three directions using three sets of mutually orthogonal ball screw and nut mechanisms. The attitude adjustment mechanism controls the pitch angle of the end effector with a two-joint rotating motor to achieve 4-degree-of-freedom movement. In the spraying process, the first ball screw group of mobile mechanism controls the horizontal movement to implement the conventional spraying action. In the process of moving, the rotating component is controlled to swing the cycle so that the spraying trajectory is sinusoidal and the sweeping action can be implemented.

The main components of the SFSC are shown in Fig. 2. The displacement mechanism is used to spatially move the spraying port of the gun mechanism to control the spraying port and have it align with the product to be sprayed for uniform spraying.

The attitude adjustment mechanism at the end of the displacement mechanism can be equated to a double-jointed robot to control the attitude of the end effector so as to be able to drive the spraying port to fine-tune the attitude in space to meet the spraying attitude requirements. Six-dimensional force sensors are added at the end (Z. Wang et al., 2024; et al., Khan, 2023) to collect the operator’s forces and moments in the  $x$ ,  $y$ , and  $z$  directions in the spatial coordinate system of the manipulator in real time, providing complete force sensing information of the object in three-dimensional space. Based on the intelligent primary–secondary real-time control teach system, the motion commands are sent to the SFSC. According to different control strategies, the corresponding motion to reach the teach point can be implemented. Dynamic calibration of a six-dimensional force transducer is used to obtain the gun position during spraying and to fit the data prediction.

The spray gun mechanism contains hoses for connecting the storage tank, air pump and spray gun made of stainless

steel. And there is a groove in the front of spray gun to retain paint residue.

The main framework of the frame mechanism is made of aluminum profile, and the box shell is fixed to the frame by bolts and nuts. An upright retractable support column is fixed at each of the four corners. The four sides of the box are equipped with auxiliary support rods to form auxiliary support. Thus, a stable operating platform is formed.

The industrial controller is equipped with the Windows 10 IoT Enterprise Edition operating system and Intel Core i5 sixth-generation CPU processor, with a touch screen, built-in demonstration software and programming software Pycharm using Python to design the program.

In the actual spraying process, the proper spraying trajectory is kept perpendicular to the surface of the workpiece. When spraying, the distance between the spray gun and the sprayed surface is generally 15–30 cm according to the angle of the coated surface. For wetter, darker and thicker coats, the distance should be closer, and for drier, lighter and thinner coats, the distance should be farther away. If the gun is tilted and runs in a circular arc or if the speed of movement is variable, a film of uniform thickness cannot be obtained while streaks and marks are easily produced. If the operating speed of the spray gun is excessively slow (below  $30 \text{ cm s}^{-1}$ ), it is susceptible to generating sagging (Geng et al., 2022).

However, in practice, after the operator has performed the force-guided demonstration, the attunement mechanism produces a large error in the reproduction process, which has the characteristics of a steady-state error. The actual spraying area deviates from the set spraying area in the  $y$  direction, which can be seen from the spraying traces.

The calculation of the linear moving mechanism is straightforward because of the motor and the screw rotating at the same speed. Thus, the displacement of  $y$  direction is linearly related to the rotation angle of the motor (D. Song et al., 2024):

$$d = 4n \times a, \tag{1}$$

where  $d$  is the wire rod stroke in millimeters and  $n$  is the guide stroke in millimeters,  $a$  is the ratio of the rotation angle of the screw to the circumference.

The speed in the  $y$  direction is also linearly related to the speed of the motor:

$$v = P \times n, \tag{2}$$

where  $v$  is the wire rod stroke in  $\text{mm min}^{-1}$ ,  $n$  is the rotational speed in  $\text{rad min}^{-1}$  and  $P$  is the guide range in  $\text{mm rad}^{-1}$ .

Troubleshooting was performed for the screw motors, and each motor was able to rotate normally. The speed and angle of rotation are as expected, and the operating current and voltage are within normal limits. Therefore, stable and accurate movement of the screw motor system was ensured so that the possibility of errors generated by the linear moving mechanism was excluded (Wang et al., 2022).

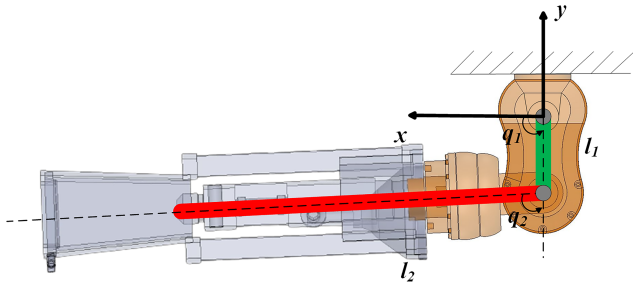


Figure 3. Schematic diagram of attitude adjustment mechanism.

It is obtained that the error in the process of machine reproduction mainly arose in the attitude adjustment mechanism, so the dynamics modeling was carried out to analyze the problems in the attitude adjustment mechanism.

### 2.2 Modeling of the dynamics of the attitude adjustment mechanism

The weight of the groove at the front of spray gun is light so that the center of mass of the spray gun mechanism is located at the back. After calculation, the simplified uniform rod length is 250 mm.

The posturing mechanism has two links and can be reduced to a standard two-jointed robotic arm (Al Juboori et al., 2024). The first link,  $l_1 = 50$  mm, is connected to the fuselage. The second link,  $l_2 = 250$  mm, is connected to the gun. The angle of rotation of the first rod with respect to the  $y$  axis is  $q_1$ , which has a range of values from 0 to  $180^\circ$ . The angle of turn of the first rod with respect to the second rod is  $q_2$ , which also has a range of values from 0 to  $180^\circ$ . The modeling process is detailed in Sect. S2 in the Supplement. The preliminary problem is judged to be the difficulty in achieving the required accuracy of conventional controls, such as sliding mode and adaptive tracking control.

For a rigid robot with  $n$  rotational joints, the dynamics can be described by a second-order nonlinear differential equation of the following form:

$$M(q)\ddot{q} + V(q, \dot{q})\dot{q} + G(q) = u + D(t), \tag{3}$$

where  $D(t) = d(t) - \Delta M(q)\ddot{q} - \Delta V(q, \dot{q})\dot{q} - \Delta G(q)$  and  $t$  represents the system running time.  $q, \dot{q}, \ddot{q} \in \mathbb{R}^n$  represent the joint angular position vector, velocity vector and acceleration vector, respectively.  $M(q), V(q, \dot{q})$  and  $G(q)$  are the nominal model parameters of the robot system.  $M(q) \in \mathbb{R}^{n \times n}$  is the robot inertia matrix.  $V(q, \dot{q}) \in \mathbb{R}^n$  represents the centrifugal and Coriolis force matrix for robotic arms.  $G(q) \in \mathbb{R}^n$  represents the gravity term.  $\Delta M(q), \Delta C(q, \dot{q})$  and  $\Delta G(q)$  are the modeling error.  $D(t) \in \mathbb{R}^n$  is the modeling error and external disturbance, and  $u \in \mathbb{R}^n$  is the control torque (Wang and Yang, 2017).  $V(q, \dot{q})\dot{q}$  represents the centrifugal and Coriolis force.

For a multi-joint robot described by Eq. (3), it generally has the following properties:

**Property 1**  $M(q)$  is a positive definite symmetric array that is bounded, and its inverse matrix exists. Namely, there exist positive numbers  $M_{\min}$  and  $M_{\max}$  such that the following equation holds:

$$0 < M_{\min} \leq M_q \leq M_{\max}. \tag{4}$$

**Property 2** The inertia matrix and the centrifugal and Coriolis forces fulfill the following relationship:

$$\dot{q}^T (\dot{M}(q) - 2V(q, \dot{q}))\dot{q} = 0. \tag{5}$$

By shifting the terms, Eq. (3) can be expressed as follows:

$$\begin{aligned} \ddot{q} &= f(q, \dot{q}) + g(q)u + g(q)D(t), \\ f(q, \dot{q}) &= -M^{-1}(q) [V(q, \dot{q})\dot{q} + G(q)], \\ M^{-1}(q) &= g(q). \end{aligned} \tag{6}$$

Generally, it can be assumed that

$$\|D(t)\| < b_0 + b_1\|q\| + b_2\|\dot{q}\|, \tag{7}$$

where  $b_0, b_1$  and  $b_2$  are positive constants.

## 3 Controller design

### 3.1 Actuator fault models

Consider the actuator fault model 1 to be as follows:

$$v(u) = \omega u + \epsilon, \tag{8}$$

where  $u$  and  $v(u)$  denote the input and output signals of the actuator, respectively, and  $\omega$  and  $\epsilon$  denote the actual control efficiency and deviation of the actuator, respectively.

**Assumption 1** There exists an unknown positive number  $\bar{\epsilon}$  such that  $|\epsilon| \leq \bar{\epsilon}, 0 < \omega \leq 1$  (Ni and Shi, 2020).

**Remark 1** In fault-tolerant control methods, Assumption 1 is often utilized to ensure that the system is controllable in the event of an actuator failure. In the robot system, due to the aging of components, damage or screw-off, it is easy to induce the actuator failure, which results in the jamming, trembling or even burning of the motor. Therefore, it is of great importance to consider possible actuator failures when designing a control law. Depending on the value of  $\omega$  and  $\epsilon$ , Eq. (8) can be categorized into the following four cases:

- $\omega = 1$  and  $\epsilon = 0$  indicates that the actuator is not malfunctioning.
- When  $0 < \underline{\omega} \leq \bar{\omega} < 1$  and  $\epsilon = 0$ , where  $\underline{\omega}$  and  $\bar{\omega}$  are unknown positive numbers, a reduction in the control effectiveness of the actuator occurs.
- $\omega = 1$  and  $\epsilon \neq 0$  indicates actuator deviation.
- When  $0 < \underline{\omega} \leq \bar{\omega} < 1, \epsilon \neq 0$ , reduced control effectiveness and deviation of the actuator occur at the same time.

### 3.2 Predefined-time tracking control

Predefined-time tracking control is a control method in which the convergence time is explicitly included in the control law, and its advantages over fixed time tracking control are that the convergence time can be set more easily without complicated calculations to get the convergence time of the system (Fei and Wang, 2019). In addition, there is no need to include the fractional order term of the tracking error in the predefined-time controller, which naturally eliminates the singular-value problem arising from the derivation of the virtual control law in fixed-time backstepping control. Predefined-time control is usually implemented based on improved preset performance functions. Another difference from fixed-time control is that predefined-time control allows for the convenient presetting of transient control performance and steady-state control performance.

**Lemma 1** For any variables  $\sigma > 0$  and  $\zeta \in \mathbb{R}$ , there exists a constant such that the following inequality holds (Xu and Zhan, 2021):

$$0 \leq |\zeta| - \zeta \tanh \frac{\zeta}{\sigma} \leq \kappa \sigma. \tag{9}$$

**Definition 1** A smooth function  $\rho(T)$  that satisfies the following conditions is called a predefined-time function:

- a.  $\rho(T)$  is a positive function.
- b. The derivative  $\dot{\rho} \leq 0$  of  $\rho(T)$  is a non-increasing function.
- c. For any  $t > T$ , there is  $\lim_{t \rightarrow T} \rho(t) = \rho(T)$ ,  $\rho(t) = \rho(T)$ , where  $T$  denotes the stabilization time of the control system.

Based on Definition 1, the following predefined-time function is proposed in this chapter:

$$\rho(t) = \begin{cases} \coth\left(r + 1 - \frac{T}{T-t}\right) - 1 + \rho(T) & \text{where } 0 \leq t < T, \\ \rho(T) & \text{otherwise,} \end{cases} \tag{10}$$

### 3.3 PRC controller design

The principle of the radial basis function (RBF) neural network fitting the unknown function  $f$  is described in Sect. S2.

The multi-joint robot dynamics model of Eq. (6) is used.

$$\ddot{q} = f(q, \dot{q}) + g(q)u + g(q)D(t)$$

Defining  $p(t) = \frac{e(t)}{\rho(t)}$ ,  $x_1 = q$  and  $x_2 = \dot{q}$ , the system (Eq. 6) can be rewritten as follows:

$$\begin{cases} \dot{x}_1 = x_2, \\ \dot{x}_2 = f(x, t) + g(x_1)v(u) + g(x_1)D(t), \\ y = x_1, \\ f(q, \dot{q}) = -M^{-1}(q)[V(q, \dot{q})\dot{q} + G(q)], \\ M^{-1}(q) = g(q). \end{cases} \tag{11}$$

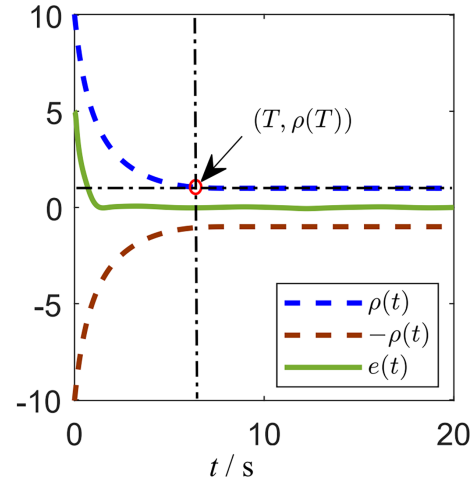


**Figure 4.** Convergence performance of the preset performance function at a predefined time.

The error transformation function is defined as

$$p(p) = \frac{p}{1-p^2},$$

where  $p = p(t)$ .

The unknown nonlinear function  $F_1$  is estimated using the RBF neural network system and denoted as follows:

$$F_1 = W_1^T S_1(x, t) + \phi_1(x, t), \tag{12}$$

where  $x = [x_1, x_2, \dot{y}_d]^T$ .

According to Assumption 1 ( $\omega_1$  and  $\epsilon_1$  are unknown), in order to improve the robustness of the system to faults, the upper and lower bounds of the fault parameters are defined as

$$\underline{\omega}_1 = \inf(E_1 g_1 \omega), \hat{\vartheta}_1 = \frac{1}{\underline{\omega}_1}, \hat{\xi}_1 = \sup(E_1 g_1 \epsilon_1). \tag{13}$$

Adaptive laws can be designed as follows:

$$\dot{\hat{l}}_1 = \frac{\mu_1 z_1^T S_1^T S_1 z_1}{4T} - \Gamma_1 \hat{l}_1, \tag{14}$$

$$\dot{\hat{\xi}}_1 = r_1 z_1 \tanh\left(\frac{z_1}{a_1}\right) - b_1 \hat{\xi}_1, \tag{15}$$

$$\dot{\hat{\vartheta}}_1 = -c_1 \hat{\vartheta}_1, \tag{16}$$

where  $a_1 > 0$ ,  $b_1 > 0$  and  $c_1 > 0$  are the design parameters.

The unknown nonlinear function  $F_2$  is estimated using the RBF neural network system, denoted as follows:

$$F_2 = W_2^T S_2(x, t) + \phi_2(x, t), \tag{17}$$

where  $x = [x_1, x_2, \dot{y}_d]^T$ .

According to Assumption 1 ( $\omega_2$  and  $\varepsilon_2$  are unknown), the upper and lower bounds of the fault parameters are defined as

$$\underline{\omega}_2 = \inf(E_2 g \omega) \vartheta_2 = \frac{1}{\underline{\omega}_2}, \tag{18}$$

$$\hat{\xi}_2 = \sup(E_2 g \varepsilon_2), \tag{19}$$

Intermediate control laws can be designed as follows:

$$\bar{u} = k_2 z_2 + \frac{z_2 \hat{l}_2 S_2^T S_2}{4T} + \hat{\xi}_2 \tanh\left(\frac{z_2}{a_2}\right). \tag{20}$$

Adaptive laws can be designed as follows:

$$\dot{\hat{l}}_2 = \frac{\mu_2 z_2^T S_2^T S_2 z_2}{4T} - \Gamma_2 \hat{l}_2,$$

$$\dot{\hat{\xi}}_2 = r_2 z_2 \tanh\left(\frac{z_2}{a_2}\right) - b_2 \hat{\xi}_2,$$

$$\dot{\hat{\vartheta}}_2 = l_2 z_2 \bar{u} - c_2 \hat{\vartheta}_2,$$

where  $a_2 > 0$ ,  $b_2 > 0$  and  $c_2 > 0$  are the design parameters.

The actual controller of PRC is designed as follows:

$$u = (g^{-1}) \left( -F_1 - F_2 - \frac{z_2 \hat{\vartheta}_2^2 \bar{u}^2}{\sqrt{z_2^T \hat{\vartheta}_2^T \bar{u}^T u \hat{\vartheta}_2 z_2 + \sigma_2}} \right),$$

where  $\sigma_2 > 0$  is a design parameter which serves to avoid the singular value problem.

### 3.4 Stability analysis

The construction method of the Lyapunov function in this article is detailed in Sect. S3 of the Supplement. Take the Lyapunov function to be

$$V = \bar{V}_1 + \bar{V}_2. \tag{21}$$

The derivation of  $V$  is obtained from Eqs. (39) and (61) in Sect. S3 in the Supplement as follows:

$$\begin{aligned} \dot{V} \leq & -k_2 z_2^T z_2 - \frac{1}{2\mu_1} \Gamma_1 \tilde{g} \tilde{l}_1^T \tilde{l}_1 - \frac{1}{2\mu_2} \Gamma_2 \tilde{g} \tilde{l}_2^T \tilde{l}_2 \\ & - \frac{1}{2r_1} b_1 \tilde{\xi}_1^T \tilde{\xi}_1 - \frac{1}{2r_2} b_2 \tilde{\xi}_2^T \tilde{\xi}_2 - \frac{1}{2l_1} \omega_1 c_1 \tilde{\vartheta}_1^T \tilde{\vartheta}_1 \\ & - \frac{1}{2l_2} \omega_2 c_2 \tilde{\vartheta}_2^T \tilde{\vartheta}_2 + \frac{1}{2\mu_1} \Gamma_1 \tilde{g} \tilde{l}_1^T \tilde{l}_1 + \frac{1}{2\mu_2} \Gamma_2 \tilde{g} \tilde{l}_2^T \tilde{l}_2 \\ & + \frac{1}{2l_1} \omega_1 c_1 \tilde{\vartheta}_1^T \tilde{\vartheta}_1 + \frac{1}{2l_2} \omega_2 c_2 \tilde{\vartheta}_2^T \tilde{\vartheta}_2 \\ & + \frac{1}{2r_1} b_1 \xi_1^T \xi_1 + \frac{1}{2r_2} b_2 \xi_2^T \xi_2 + 2T + \frac{1}{2} \phi_1^T \phi_1 \\ & + \frac{1}{2} \phi_2^T \phi_2 + \sigma_2 \omega_2 + 0.2785 a_1 \xi_1 + 0.2785 a_2 \xi_2. \end{aligned}$$

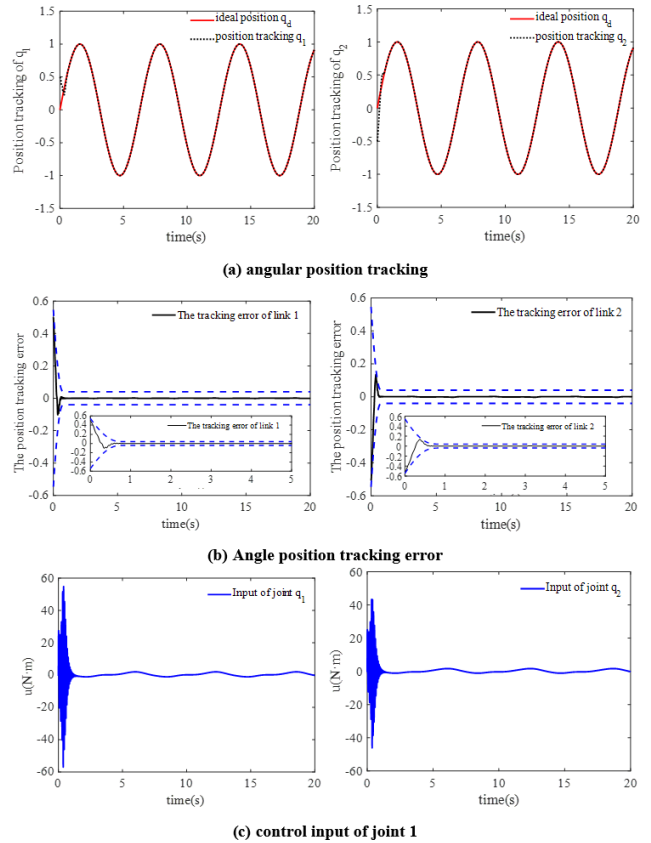


Figure 5. Robot joint of the attitude adjustment mechanism.

From this, it is concluded that

$$\dot{V} \leq -kV + C, \tag{22}$$

where  $k = \min\{2k_2, \Gamma_1, \Gamma_2, b_1, b_2, c_1, c_2\}$  and  $C = \frac{1}{2\mu_1} \Gamma_1 \tilde{g} \tilde{l}_1^2 + \frac{1}{2\mu_2} \Gamma_2 \tilde{g} \tilde{l}_2^2 + \frac{1}{2l_1} \omega_1 c_1 \tilde{\vartheta}_1^2 + \frac{1}{2l_2} \omega_2 c_2 \tilde{\vartheta}_2^2 + \frac{1}{2r_1} b_1 \tilde{\xi}_1^T \tilde{\xi}_1 + \frac{1}{2r_2} b_2 \tilde{\xi}_2^T \tilde{\xi}_2 + T_1 + T_2 + \frac{1}{2} \phi_1^T \phi_1 + \frac{1}{2} \phi_2^T \phi_2 + \sigma_2 \omega_2 + 0.2785 a_1 \xi_1 + 0.2785 a_2 \xi_2$ . Integrating both sides of Eq. (17) yields

$$V \leq V(0) + \frac{C}{k}.$$

Combining Eqs. (29) and (51) in Sect. S3 of the Supplement yields that the conversion error converges to the following tight set:

$$z_1 \leq \sqrt{2V(0) + \frac{C}{k}} z_2 \leq \sqrt{2V(0) + \frac{C}{k}}.$$

According to Eqs. (29) and (51) in Sect. S3 of the Supplement, the estimation error will converge to the following compact set:

$$\left\{ \begin{aligned} \tilde{l}_1 &\leq \sqrt{2\mu_1(V(0) + \frac{C}{k})} \\ \tilde{l}_2 &\leq \sqrt{2\mu_2(V(0) + \frac{C}{k})} \end{aligned} \right\}, \left\{ \begin{aligned} \tilde{\vartheta}_1 &\leq \sqrt{\frac{2l_1}{\omega_1}(V(0) + \frac{C}{k})} \\ \tilde{\vartheta}_2 &\leq \sqrt{\frac{2l_2}{\omega_2}(V(0) + \frac{C}{k})} \end{aligned} \right\}. \tag{23}$$

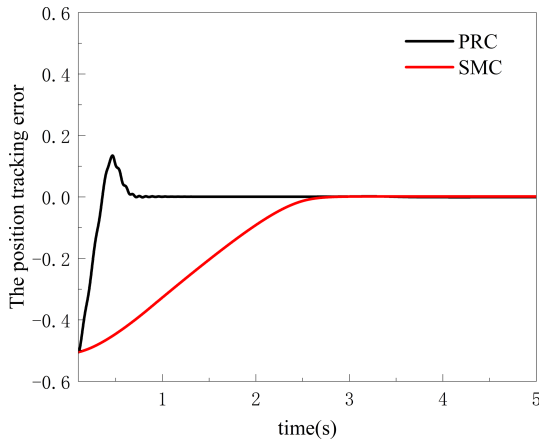


**Figure 6.** Comparison between convergence performance and traditional methods.

Therefore, all signals of the closed-loop system are bounded. According to Eqs. (29) and (30) in Sect. S3, it can be seen that the position tracking error and angular velocity tracking error converge to the preset compact set within time. Predefined-time control functions (Eq. 10) needs to be adopted, and the condition of  $|z(0)| \leq \rho(0)$  needs to be guaranteed. Then, during the operation of the system, the overshoot of both the position tracking error and the velocity tracking error will not exceed the boundary of the performance function, thus ensuring that the system converges according to the preset accuracy. In this case,  $\dot{V} < 0$ . Therefore, this control law satisfies the arrival condition of SMC, and the control system is stable (Qian et al., 2024; Kim and Suh, 2024; Tang et al., 2022).

#### 4 Simulation verification results and analysis

In order to demonstrate the effectiveness of the proposed method, the PRC method considering actuator faults is applied to the attitude adjustment mechanism of SFSC.

For the above algorithm, a multiple-in, multiple-out (MIMO) dynamics model (Deng et al., 2024) of the attitude adjustment mechanism is adopted for simulation studies:

$$M(q)\ddot{q} + V(q, \dot{q})\dot{q} + G(q) = u + D(t). \tag{24}$$

The state quantities in the mechanism are, respectively, as follows:

$$M(x_1) = \begin{bmatrix} M_{11} & M_{12} \\ M_{21} & M_{22} \end{bmatrix}, C(x_1, x_2) = \begin{bmatrix} C_{11} & C_{12} \\ C_{21} & 0 \end{bmatrix},$$

$$G(x_1) = \begin{bmatrix} G_1 \\ G_2 \end{bmatrix},$$

where  $M_{11} = m_1 l_1^2 + m_2 (l_1^2 + l_2^2 + 2l_1 l_2 \cos q_2)$ ,  
 $M_{12} = M_{21} = m_2 (l_2^2 + l_1 l_2 \cos q_2)$ ,  $M_{22} = m_2 l_2^2$ ,  
 $C_{11} = -m_2 l_1 \dot{q}_2 \sin q_2$ ,  $C_{12} = -m_2 l_1 \sin q_2 (\dot{q}_1 + \dot{q}_2)$ ,

$C_{21} = m_2 l_1 q_1 \sin q_2$ ,  $G_1 = (m_1 + m_2) \times l_1 \cos q_2 + m_2 l_2 \cos(q_1 + q_2)$ ,  $G_2 = m_2 l_2 \cos(q_1 + q_2)$ ,  $m_1 = 1$  kg,  $m_2 = 2.1$  kg,  $l_1 = 0.1$  m and  $l_2 = 0.4$  m. The initial state of the system is  $q_1 = 0.5$  rad,  $\dot{q}_1 = 0$  rad s<sup>-1</sup>,  $q_2 = -0.5$  rad,  $\dot{q}_2 = 0$  rad s<sup>-1</sup>.

The desired trajectory of the system is

$$q_{d1} = \cos(\pi t), q_{d2} = \cos(\pi t).$$

The controller parameters are set to

$$k_1 = k_2 = \mu_1 = \mu_2 = r_1 = r_2 = l_1 = l_2 = 1,$$

$$T_1 = \Gamma_1 = \Gamma_2 = c_1 = c_2 = b_1 = b_2 = 0.1.$$

We assume that actuator fault 1 of the SFSC occurs in the form

$$D(t) = [\dot{q}_1(t) + 0.1 \sin(\dot{q}_1(t))\dot{q}_2(t) + 0.1 \sin(\dot{q}_2(t))]^T,$$

and actuator fault 2 of the spraying robot occurs at  $t = 10$  s as follows:

$$v(u) = 0.8u - [0.1 \quad 0.1]^T.$$

The predefined-time function can be designed as

$$\rho(t) = \begin{cases} \coth\left(-\frac{1}{1-t} + 1.8\right) - 0.96 & \text{when } 0 \leq t < 1, \\ 0.04 & \text{otherwise,} \end{cases}$$

where the initial value of the neural network weights is taken as 0.1. The center vector of the hidden layer,  $c$ , is given as  $[-2 \quad -1 \quad 0 \quad 1 \quad 2]$ . The width of the Gaussian basis function is taken to be  $b = 3$ .

The control law of PRC utilizes Eq. (19).

Figure 5a and b show the plots of joint position tracking performance, joint position tracking error for the attitude adjustment mechanism under actuator failure and uncertainty and time-varying external perturbation conditions, respectively.

From the joint position tracking curves of the attitude adjustment mechanism in Fig. 5a, it can be seen that joint position  $q_1$  can quickly track the target trajectory,  $q_{d1}$ , within 0.5 s, and joint position  $q_2$  can also quickly track the target trajectory,  $q_{d2}$ , within 0.5 s. The verified that the PRC controller still has good position tracking and speed tracking performance under the influence of fault uncertainties.

The simulation results in Fig. 5b show that the output of the PRC controller designed in this chapter enables the joint position and velocity tracking errors to converge to 0 within a finite time.

Figure 5c shows the control inputs of attitude adjustment mechanism with an initial input of 40 N m and a steady-state input of 2 N m.

It can be found more intuitively by comparing the traditional backstepping SMC method (Z. Song et al., 2024), and the tracking error can be guaranteed to converge quickly, satisfying the specified performance within a preset time of

**Table 1.** Comparison between convergence performance and traditional methods.

Method	Convergence time, $t_r$ [s]	Initial error, $e$ [rad]	Steady-state error, $e$ [rad]	Control input, $u$ [N m]	Initial input, $u$ [N m]
PRC	0.41 s	-0.47	0.01	2.14	42.34
SMC	3.12 s	-0.50	0.02	2.45	163.23

$T_s = 1$  s using the method in this paper. The convergence time is improved from 3.12 s in SMC to within 1 s, and almost the same steady-state error can be achieved; the initial torque is reduced from 163.23 to 42.34 N m, which greatly reduces the load required to start the motor, and the steady-state error is almost zero.

In summary, the simulation results show that the control system has good tracking performance and improves the control accuracy.

## 5 Conclusions

In this paper, the PRC method considering actuator fault for controlling unknown Euler–Lagrange systems was proposed, which is applied to control the attitude adjustment mechanism of the SFSC robot for vehicle surface repair. A preset performance function is proposed, and its continuity, convergence and strict positivity are proven. The control method is validated by simulation to effectively control the position and velocity of the robot joints under actuator failure and uncertainty and time-varying external perturbation conditions, which improves the convergence speed to within 1 s. By comparing it with a traditional SMC, the improvement in control accuracy and convergence speed has been verified. This control strategy can be applied to the SFSC with the potential to improve its performance and reliability. PRC can be combined with techniques such as deep reinforcement learning (DRL) control, event-triggered control and model predictive control, which are applied in different scenarios. In the future, the application of PRC technology to other complex intelligent agent structures will be a worthwhile research direction.

**Code availability.** This code is the core competitiveness of our research team, and according to regulations, our code is confidential. The data is not publicly available.

**Data availability.** The data is not publicly available.

**Supplement.** The supplement related to this article is available online at: <https://doi.org/10.5194/ms-16-51-2025-supplement>.

**Author contributions.** JZ: conceptualization, methodology, software, investigation, formal analysis and writing (original draft). YinL: data curation, resources and supervision. BP: visualization, investigation and supervision. YiW: resources, funding acquisition and supervision. ZY: software, validation and writing (review and editing). ZD: visualization and writing (review and editing).

**Competing interests.** The contact author has declared that none of the authors has any competing interests.

**Disclaimer.** Publisher's note: Copernicus Publications remains neutral with regard to jurisdictional claims made in the text, published maps, institutional affiliations, or any other geographical representation in this paper. While Copernicus Publications makes every effort to include appropriate place names, the final responsibility lies with the authors.

**Acknowledgements.** First of all, we are grateful to the National Key Lab of Aerospace Power System and Plasma Technology for providing experimental equipment and financial support, which provided a solid foundation for our research. We are grateful for the cooperation of China Aerodynamics Research and Development Center High Speed Institute and Hefei University of Technology, whose expertise and resources contributed greatly to our research. Finally, we thank the reviewers and editors for their hard work and valuable comments, and their suggestions greatly improved the quality of our paper.

**Financial support.** This project was supported by the National Major Science and Technology Projects of China (grant no. J2019-V-0008-0102), National Key Lab of Aerospace Power System (grant no. APSPT202303002), Plasma Technology foundation, and Shaanxi Provincial Innovation 10 Capacity Support program (grant no. 2023-CX-TD-22).

**Review statement.** This paper was edited by Daniel Condurache and reviewed by two anonymous referees.

## References

- Al Juboori, A. M., Hussein, M. T. and Qanber, A. S. G.: Swing-up control of double-inverted pendulum systems, *J. Mech. Sci.*, 15, 47–54, <https://doi.org/10.5194/ms-15-47-2024>, 2024.
- Becerra, H. M., Vázquez, C. R., Arechavaleta, G. and Delfin, J.: Predefined-time convergence control for high-order integrator systems using time base generators, *J. IEEE T. Contr. Syst. T.*, 26, 1866–1873, <https://doi.org/10.1109/TCST.2017.2734050>, 2018.
- Chen, W., Li, X., Ge, H., Wang, L. and Zhang, Y.: Trajectory planning for spray painting robot based on point cloud slicing technique, *J. Electronics*, 9, 908, <https://doi.org/10.3390/electronics9060908>, 2020.
- Deng, X., Chen, H. and Li, L.: Improved Fixed Time Preset Performance Sliding Mode Control for Robotic Manipulator, *IEEE, ICIT 2024*, 1–6, 2024.
- Fei, J. and Wang, T.: Adaptive fuzzy-neural-network based on RBFNN control for active power filter, *J. Int. J. Mach. Learn. Cyb.*, 10, 1139–1150, <https://doi.org/10.1007/s13042-018-0792-y>, 2019.
- Geng, G., Jiang, F., Chai, C., Wu, J., Zhu, Y., Zhou, G. and Xiao, M.: Design and experiment of magnetic navigation control system based on fuzzy PID strategy, *J. Mech. Sci.*, 13, 921–931, <https://doi.org/10.5194/ms-13-921-2022>.
- He, Y., Zhou, Y., Cai, Y., Yuan, C., and Shen, J.: DSC-based RBF neural network control for nonlinear time-delay systems with time-varying full state constraints, *J. ISA Trans.*, 129, 79–90, <https://doi.org/10.1016/j.isatra.2021.12.010>, 2022.
- Khan, S. G.: Adaptive chaos control of a humanoid robot arm: a fault-tolerant scheme, *J. Mech. Sci., Mech. Sci.*, 14, 209–222, <https://doi.org/10.5194/ms-14-209-2023>, 2023.
- Kim, S. J. and Suh, J. H.: Model-Free RBF Neural Network Intelligent-PID Control Applying Adaptive Robust Term for Quadrotor System, *J. Drones*, 8, 179, <https://doi.org/10.3390/drones8050179>, 2024.
- Lai, G., Zou, S., Xiao, H., Wang, L., Liu, Z. and Chen, K.: Fixed-time adaptive fuzzy control with prescribed tracking performances for flexible-joint manipulators, *J. Franklin I.*, 361.7, 106809, <https://doi.org/10.1016/j.jfranklin.2024.106809>, 2024.
- Li, K., Hua, C., You, X., and Ahn, C. K.: Output feedback predefined-time bipartite consensus control for high-order nonlinear multiagent systems, *J. IEEE T. Circuits-I.*, 68, 3069–3078, <https://doi.org/10.1109/TCSI.2021.3071974>, 2021.
- Liu, Y., Zi, B., Wang, Z., Qian, S., Zheng, L., and Jiang, L.: Adaptive lead-through teaching control for spray-painting robot with closed control system, *J. Robotica*, 41, 1295–1312, <https://doi.org/10.1017/S0263574722001710>, 2023.
- Lynch, K. M. and Park, F. C.: *Modern robotics*, M. C.U.P., 2017.
- Morelli, U., Dalla Vedova, M.D. and Maggiore, P.: *Automatic painting and paint removal system – A preliminary design for aircraft applications*, C. Springer International Publishing. (RAAD 2018), pp. 640-650. 2018.
- Munoz-Vazquez, A. J., Sánchez-Torres, J. D., Jimenez-Rodriguez, E., and Loukianov, A. G.: Predefined-time robust stabilization of robotic manipulators, *J. IEEE-ASME T. Mech.*, 24, 1033–1040, <https://doi.org/10.1109/TMECH.2019.2906289>, 2019.
- Ni, J. and Shi, P.: Global predefined time and accuracy adaptive neural network control for uncertain strict-feedback systems with output constraint and dead zone, *J. IEEE SMCA*, 51, 7903–7918, <https://doi.org/10.1109/TSMC.2020.2994808>, 2020.
- Pan, Y., Ji, W., Lam, H. K., and Cao, L.: An improved predefined-time adaptive neural control approach for nonlinear multiagent systems, *J. IEEE T. Autom. Sci. Eng.*, 4, 6311–6320, <https://doi.org/10.1109/TASE.2023.3324397>, 2023.
- Qian, S., Zhang, J., Pei, Z., Sun, X. and Wu, Z.: Development of a flexible endoscopic robot with autonomous tracking control ability using machine vision and deep learning, *J. Mech. Sci.*, 15, 223–236, <https://doi.org/10.5194/ms-15-223-2024>, 2024.
- Song, D., Xiao, X., Ma, J., and Zhang, L.: Modeling and control system experiment of a novel series three-axis stable platform, *Mech. Sci.*, 15, 209–221, <https://doi.org/10.5194/ms-15-209-2024>, 2024.
- Song, Z., Bao, D., Wang, W., and Zhao, W.: Adaptive Dynamic Boundary Sliding Mode Control for Robotic Manipulators under Varying Disturbances, *J. Electronics*, 13, 900, <https://doi.org/10.3390/electronics13050900>, 2024.
- Spong, M. W., Hutchinson, S., and Vidyasagar, M.: *Robot modeling and control*, M. John Wiley & Sons, 2020.
- Tang, C., Huang, Z., Wei, C., and Zhao, Y.: Dynamic and sliding mode control of space netted pocket system capturing and attitude maneuver non-cooperative target, *Mech. Sci.*, 13, 751–760, <https://doi.org/10.5194/ms-13-751-2022>, 2022.
- Tang, L. and Zhao, J.: Neural network based adaptive prescribed performance control for a class of switched nonlinear systems, *J. Neurocomputing*, 230, 316–3621, <https://doi.org/10.1016/j.neucom.2016.12.011>, 2017.
- Wang, B., Lei, Y., Fu, Y., and Geng, X.: Autonomous vehicle trajectory tracking lateral control based on the terminal sliding mode control with radial basis function neural network and fuzzy logic algorithm, *Mech. Sci.*, 13, 713–724, <https://doi.org/10.5194/ms-13-713-2022>, 2022.
- Wang, C., Guo, Q., Wang, J., Liu, Z., and Chen, C. P.: Fixed-time fuzzy control for uncertain nonlinear systems with prescribed performance and event-triggered communication, *J. IEEE T. Circuits-I.*, 71, 2362–2371, <https://doi.org/10.1109/TCSI.2024.3371050>, 2024.
- Wang, M. and Yang, A.: Dynamic learning from adaptive neural control of robot manipulators with prescribed performance, *J. IEEE SMCA*, 47.8, 2244–2255, <https://doi.org/10.1109/TSMC.2016.2645942>, 2017.
- Wang, Z., Mei, L., and Ma, X.: A novel generalized sliding mode controller for uncertain robot manipulators based on motion constraints, *Mech. Sci.*, 15, 55–62, <https://doi.org/10.5194/ms-15-55-2024>, 2024.
- Xu, Q. and Zhan, Q.: A real-time inverse kinematics solution based on joint perturbation for redundant manipulators, *Mech. Sci.*, 12, 221–235, <https://doi.org/10.5194/ms-12-221-2021>, 2021.
- Yang, C., Li, P., Wang, Y., Ye, W., Sun, T., Huang, F., and Zhang, H.: Multi-objective optimization design of parallel manipulators using a neural network and principal component analysis, *J. Mech. Sci.*, 14, 361–370, <https://doi.org/10.5194/ms-14-361-2023>, 2023.
- Ye, D., Zou, A. M., and Sun, Z.: Predefined-time predefined-bounded attitude tracking control for rigid spacecraft, *J. IEEE T. Aero. Elec. Sys.*, 58, 464–472, <https://doi.org/10.1109/TAES.2021.3103258>, 2021.

Yu, Q., Wang, G., Hua, X., Zhang, S., Song, L., Zhang, J., and Chen, K.: Base position optimization for mobile painting robot manipulators with multiple constraints, *J. Robot Cim-Int. Manuf.*, 54, 56–64, <https://doi.org/10.1016/j.rcim.2018.05.007>, 2018.

Zhang, B., Wu, J., Wang, L., and Yu, Z.: Accurate dynamic modeling and control parameters design of an industrial hybrid spray-painting robot, *J. Robot Cim-Int. Manuf.*, 63, 101923, <https://doi.org/10.1016/j.rcim.2019.101923>, 2020.